UNIVERSITI TEKNOLOGI MARA

University Publication Centre (UPENA)

Journal of Mechanical Engineering

An International Journal

Volume 6 No. 1 **April 2009** **ISSN 1823-5514**

JOURNAL OF MECHANICAL ENGINEERING
(JMechE)

Journal of Mechanical Engineering is jointly published by the Faculty of Mechanical Engineering and University Publication Centre (UPENA), Universiti Teknologi MARA, 40450 Shah Alam, Selangor, Malaysia.

Journal of Mechanical Engineering

An International Journal

Volume 6 No. 1 **April 2009** **ISSN 1823-5514**

Dynamics and Iterative Learning Control of Robots with Parallel Kinematical Structures

Bodo Heimann[1], & Houssem Abdellatif
Leibniz University of Hannover, Institute of Robotics (IfR)
Appelstr. 11a, D-30167 Hannover, Germany
[1]heimann@ifr.uni-hannover.de

ABSTRACT

The paper deals with model-based control of robots with parallel kinematical structure (PKM). At first, an approach for the identification of friction and rigid-body dynamics of complex parallel kinematical structures is presented. The approach is based on optimal excitation trajectories. The trajectories are bounded, such they are easy to be fit into the small and hard constraint workspace of PKM. Secondly, some results are presented using feedforward control in order to compensate nonlinear dynamical influences. Thirdly, Iterative Learning Control (ILC) is proposed in this paper for tracking accuracy enhancement of a parallel direct driven manipulator. It is shown both by means of simulation study and experimental results that linear ILC is appropriate for application to the considered high nonlinear and coupled systems.

Keywords: *Parallel Kinematical Machines, Inverse Dynamics, Feedforward Compensation, Iterative Learning Control*

Introduction

Due to their precision, stiffness and dynamics parallel kinematical machines (PKM) are becoming more and more interesting in the field of machine tools and robots. Model-based control algorithms are necessary to take advantage of the possibilities offered by such structures. To utilize multibody models for control, the dynamical model must be efficiently formulated in order to meet real-time requirements. Furthermore, the model parameters like masses and moments of inertia as well as friction parameters must be known. If they are not given from design data, they have to be experimentally identified. Till now, this experimental determination is restricted to simple models and adaptive control algorithms (see [1], [2]).

In this paper we also propose the application of ILC for the control of 6-DOF parallel manipulators. This method is an additional one besides classic feedforward control. Such application is relatively new in dynamics and control of PKM. It is believed, that ILC could help an important breakthrough in the control improvement and enhancement of tracking accuracy of parallel robots. This paper will focus on the application of ILC on a linear direct driven hexapod PaLiDA in terms of simulation and experimental study, see [6]. As recommended in [12], linear first-order learning formulations and algorithms are chosen to be validated. Two approaches are investigated, a heuristic one, that do not need any explicit plant model and a second model-based algorithm.

It will be very interesting to investigate if ILC could be applied for direct driven parallel manipulators like it has been proven for classic industrial robot in [15], [16], [19]. Industrial robots are characterized by high gear ratios, such that decentralized single-joint consideration is possible. From this point of view, the studied PKM system is very different due to its mechanical coupling and the use of gearless direct drives. First, the methods are implemented in accurate simulation that enables the study of different factors, such the influence of measurement noise, log term stability, etc. The experimental evaluation on the real system follows and both approaches are compared in terms of control improvement and convergence.

Examples for Parallel Kinematical Machines :

Hydraulic Hexapod (HSP)

The hexapod HSP is a test stand to simulate vibrations and movements appearing in vehicles. The actuators are hydraulic cylinders with a maximum force of 15 kN each. To reduce forces acting in the joints the platform is a lightweight construction. Therefore, the maximal acceleration of HSP is larger than 50 g. The valves are able to realize frequencies of more than 50 Hz. The maximal speed is limited to 1 m/s by the size of the valves. Figure 1 shows the test stand both as a multibody system (MBS) model and as a physical realization. The table left to the platform is used to fix the test samples. The platform is shown in centred position. Some necessary hydraulic components like pipes and accumulators are not included in the MBS model.

Contrary to most hydraulic test beds the workspace is not limited by the hydraulic actuators. Therefore, each TCP-platform position must be checked with respect to the workspace. That means, the control unit includes some safety features, like path tracing errors and other safety functions.

The platform is used in a standard regime as a test bed for frequencies of about 10 Hz and amplitudes of about 25 mm. In applications with only small forces compared to the power of the actuators the dynamic forces have only limited influence due to the resulting low accelerations. It follows that the accuracy of the platform is mainly appointed by the accuracy of one single actuator. In

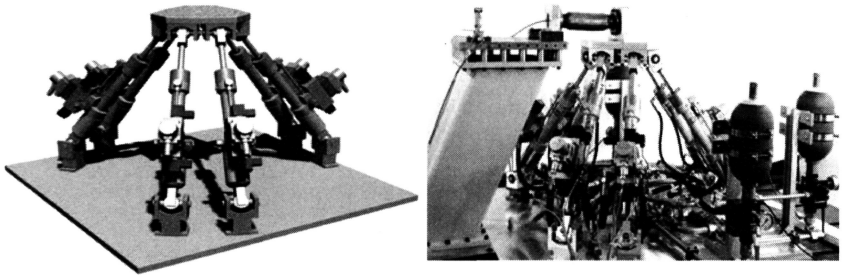

Figure 1: Hydraulic Stewart-Gough-platform:
HSP Model and Test Bed

order to reduce the path error the model of the hydraulic actuator has to be improved. Therefore, the hydraulic actuator model is more important than the dynamical ones of the parallel mechanism. That means, the control of the HSP can be reduced to a non-linear decoupled single axis controller. The actuator speed is used for a feedforward control.

Hexapod with Linear Direct Drives (PaLiDA)

The studied prototype PaLiDA is a hexapod machine that is equipped with 6 linear direct drives, see Figure 2. A commercial electromagnetic linear motor, originally designed for fast lifting movements, is the basic element for the developed actuator. To use this motor as a PKM actuator, several modifications were necessary. It had to be enhanced guidance of the slider with minimized radial backlash.

The main advantage of such drives for parallel kinematics results from the high control dynamics which cannot be achieved by conventional actuation systems. In contrast to the ball screw drive, additional mechanical wear parts are not needed, such that there is no backlash and lower inertia is guaranteed. One example for such linear drives is the LinMot-P from Sulzer, see Figure 3.

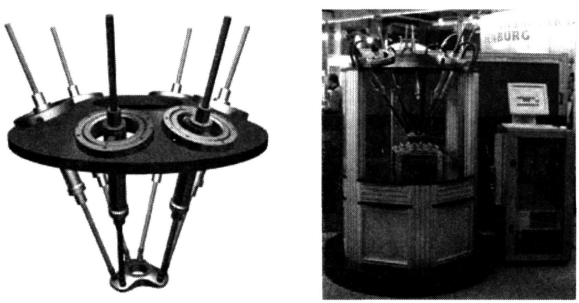

Figure 2: Hexapod PaLiDA: MBS Model and Test Bed.

It is a high dynamical electro-magnetic linear drive with acceleration up to 150m/s² and with fully integrated position sensors. Since this product has been designed for a different application it was necessary to enhance its performance for robotic applications. The motor creates high magnetic fields to move the slider, which influences the quality of the Hall sensors.

Statorhousing

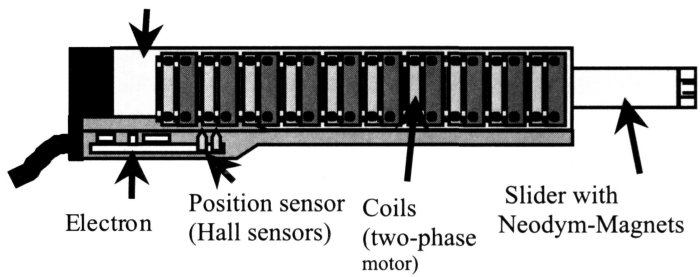

Figure 3: Linear Direct Drive (Source: Sulzer NTI)

In order to pass on additional external sensors, it was necessary to develop appropriate compensation strategies to keep adequate measurement quality, see ([6], [8]). The motor control unit was modified to allow direct force control for the actuator.

The first prototype was designed after an evaluation of different construction alternatives, see [17]. The favoured solution is a cardan joint, which encloses the motor. Its platform has to be lightweight to reduce dynamical forces.The motors are integrated in length-variable struts, see Figure 4. The motor is mounted in the centre of the upper cardan-ring which is connected to the base platform.

The joint between the slider and the moveable platform is a small universal joint. The size of the ring allows the supporting of the motor. Such concept enhances the dynamic capabilities of the machine by reducing the movable elements.

The challenging construction of a stiff connection between a long tube and the motor was another aspect. A motor housing with an integrated bearing system has been developed such it allows the integration of water cooling system.

The electronic control hardware was modified to realise a direct force control of the motor (current control), which is a necessary condition for the implementation of model-based feedforward control. Except the current control, the drive control is implemented on a DSP card including the calculation of the actuator position from the position signal of the Hall-sensors. Using a simple PID-controller and the developed compensation strategies, the positioning

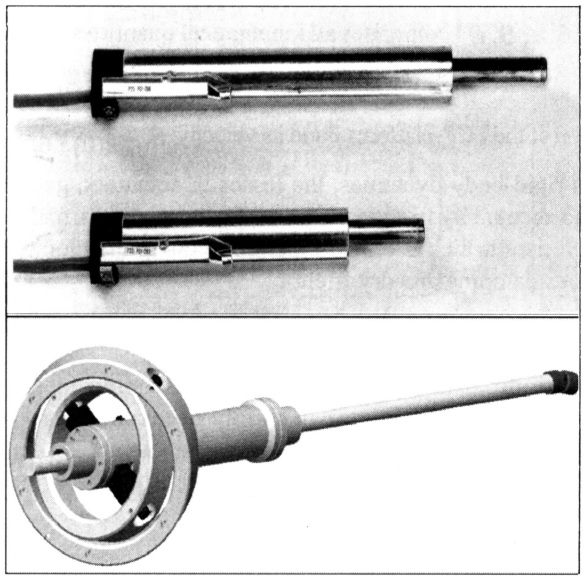

Figure 4: Single Strut with Integrated Linear Drive and Cardan Joint

accuracy of the actuator could be improved by factor 10. However, it has to be mentioned that the amount of information of the Hall-sensor is limited. An accuracy of about 20 μm can be achieved for the repeating accuracy for PTP (point-to-point) motions. Nevertheless, an external position measuring system has still to be chosen for applications that require absolute accuracy less than 100 μm. The maximum force of a single actuator is 200 N.

Modeling

Newton - Euler equations in combination with d'Alembert's or Jourdain's principle of virtual work or power are known to be highly efficient for the solution of the inverse dynamics of parallel robots, see [7]. Therefore, an approach is utilized which combines Jourdain's principle in parameter-linear form with analytical rules for the determination of the minimal parameter set, see [3].

The approach leads to very efficient C-code. It yields a formulation of the rigid-body dynamics, which is linear with respect to the base parameter vector $\boldsymbol{p}_{\mathrm{rb,min}}$ that consists of unknown and minimal inertial parameters of the mechanism

$$_{\mathrm{rb}} = \boldsymbol{A}_{\mathrm{rb}}\left(\boldsymbol{x}, \dot{\boldsymbol{\theta}}, \ddot{\boldsymbol{\theta}}\right)\boldsymbol{p}_{\mathrm{rb,min}} \tag{1}$$

where $\boldsymbol{Q}_{\mathrm{a,rb}}$ is the vector of the actuator forces caused by rigid-body dynamics.

The matrix $\boldsymbol{A}(\boldsymbol{x}, \dot{\boldsymbol{\theta}}, \ddot{\boldsymbol{\theta}})$ comprises all kinematical quantities and is a function of the generalized coordinates, velocities and accelerations. These are chosen as position and orientation of the TCP-platform $\boldsymbol{x}$ and its velocity $\dot{\boldsymbol{\theta}} = \begin{bmatrix} {}_{(0)}\boldsymbol{v}_E^T & {}_{(0)}\boldsymbol{\omega}_E^T \end{bmatrix}^T$.

Besides rigid-body dynamics, the losses in actuators, gears and bearings are taken into account by friction models. The losses are normally modeled as a force characteristic which is only a function of the joint velocity $\dot{q}_i$, e. g. by a sum of viscous damping and dry friction:

$$= r_{1,i}\dot{q}_i + r_{2,i}\text{sign}(\dot{q}_i) \tag{2}$$

These single joint friction models are not restricted to actuated joints. Friction models of passive joints can simply be taken into account by using Jourdain's principle of virtual power. With the variables of all considered joints $\boldsymbol{q}$ and the corresponding friction forces $\boldsymbol{Q}_f$, the effective actuator friction forces $\boldsymbol{Q}_{a,f}$ result in

$$_f = \left(\frac{\partial \dot{\boldsymbol{q}}}{\partial \dot{\boldsymbol{q}}_a}\right)^T \boldsymbol{Q}_f = \boldsymbol{J}^T \left(\frac{\partial \dot{\boldsymbol{q}}}{\partial \dot{\boldsymbol{\theta}}}\right)^T \boldsymbol{Q}_f \tag{3}$$

where $\dot{\boldsymbol{q}}_a$ are the velocities of the actuated joints. Thus, the effective actuator friction forces depend directly on the actual configuration $\boldsymbol{x}$ because the JACOBIAN $(\partial \dot{\boldsymbol{q}} / \partial \dot{\boldsymbol{q}}_a)^T$ is a function of $\boldsymbol{x}$. By taking into account previous equations, it is easy to formulate the effective friction forces in a parameter-linear form:

$$= \underbrace{\mathbf{J}^T \left(\frac{\partial \dot{\mathbf{q}}}{\partial \dot{\boldsymbol{\theta}}}\right)^T \begin{bmatrix} \dot{\mathbf{q}} & \text{sign}(\dot{\mathbf{q}}) \end{bmatrix}}_{A_f} \underbrace{\begin{bmatrix} \mathbf{r}_1 \\ \mathbf{r}_2 \end{bmatrix}}_{p_{f,\min}} = \mathbf{A}_f(\boldsymbol{x}, \dot{\boldsymbol{\theta}}, \ddot{\boldsymbol{\theta}}) \mathbf{p}_{f,\min} \tag{4}$$

Combining equations (1) and (4) yields the final form of the integral dynamics

$$= \mathbf{A}_{rb}(\mathbf{x}, \dot{\boldsymbol{\theta}}, \ddot{\boldsymbol{\theta}}) \mathbf{p}_{rb,\min} + \mathbf{A}_f(\mathbf{x}, \dot{\boldsymbol{\theta}}, \ddot{\boldsymbol{\theta}}) \mathbf{p}_{f,\min} = \mathbf{A}(\mathbf{x}, \dot{\boldsymbol{\theta}}, \ddot{\boldsymbol{\theta}}) \mathbf{p} \tag{5}$$

Identification Approach for the Dynamic Parameters

The main advantage of applying linear estimators is their computational efficiency. This explains their wide reputation in the identification of the dynamics for serial robotic manipulators, see [2].

For parallel structures, linear estimators have also proven their efficiency in recursive [4] as well as in the general form [10].

Linear Parameter Estimation

The formulation of the estimation problem can be derived from (5) as

$$\underbrace{\begin{bmatrix} Q_a^{(1)} \\ \vdots \\ Q_a^{(N)} \end{bmatrix}}_{\Gamma} = \underbrace{\begin{bmatrix} A\left(x^{(1)}, \dot{\theta}^{(1)}, \ddot{\theta}^{(1)}\right) \\ \vdots \\ A\left(x^{(N)}, \dot{\theta}^{(N)}, \ddot{\theta}^{(N)}\right) \end{bmatrix}}_{\Psi} p + \underbrace{\begin{bmatrix} e^{(1)} \\ \vdots \\ e^{(N)} \end{bmatrix}}_{\eta}, \quad (6)$$

with the measurement vector Γ, the information or regression matrix Ψ and the error vector η that accounts for disturbances. The formulation of PKM dynamics in a linear form reduces the system complexity to a simple LP model structure (*linear in its parameter*). The solution of the over-determined equations system (6) in a Least-Squares sense yields the estimation $\hat{p}$ of the parameter vector

$$= \min\left(\eta^T \eta\right) \quad \Rightarrow \quad \hat{p} = \left(\Psi^T \Psi\right)^{-1} \Psi^T \Gamma . \quad (7)$$

This corresponds to an upper bound for estimation uncertainty, see [8]:

$$\frac{\left\| p_{min} - \hat{p}_{min} \right\|}{\left\| p_{min} \right\|} \leq \text{cond}\ (\Psi) \frac{\left\| \eta \right\|}{\left\| \Gamma \right\|}, \quad (8)$$

where $\kappa = \text{cond}\ (\Psi) = \dfrac{\sigma_{max}(\Psi)}{\sigma_{min}(\Psi)}$ and $\sigma_{max}(\Psi), \sigma_{min}(\Psi)$ are respectively the largest and smallest singular value of the information matrix. The condition number κ can be used as a criterion for parameter excitation ([9], [10]), since it is the quotient of the largest and smallest singular values of Ψ. Its minimization yields uniform excitation of all elements of the parameter vector p and minimizes therefore the upper bound of the estimation uncertainty, equ. (8). Hence, the experiment design is the task to find a N-dimensional set of configurations (see (6)), such that the corresponding information matrix has a minimal condition number. In the case of an indirect identification approach, this set is composed of single discrete N configurations that resulted from N different and simple trajectories, see [8]. In the direct estimation the N elements of the information matrix correspond to one continuous trajectory, which has to be designed to fulfill the optimality criterion of minimal condition number. It is also very important to notice that this criterion is sensible in the deterministic framework, where the disturbances of the information matrix Ψ is assumed to be negligible in comparison to the measurement noise η.

Input-Trajectory Optimization, Design of Experiments

Generally, excitation trajectories are obtained by means of nonlinear optimization with motion constraints (e.g. joint limitation, workspace, etc.). The mathematical description of the motion is crucial for success and computational efficiency of the optimization, because the trajectory parameters are the degrees of freedom of the optimization problem. By considering $\boldsymbol{\xi}$ as the vector regrouping such parameters, a trajectory in the space of minimal coordinates can be describes as follows

$$\Im(\boldsymbol{\xi}) = \left\{ \boldsymbol{x} \in R^6, \boldsymbol{f_t}(\boldsymbol{x}, t, \boldsymbol{\xi}) = \boldsymbol{0}, \forall t \right\} \tag{9}$$

The optimal excitation trajectory has to minimize the resulted condition number and is associated with the optimal parameter set $\boldsymbol{\xi}_0$

$$\boldsymbol{\xi}_0 = \arg\min_{\boldsymbol{\xi}} \left(\text{cond}(\boldsymbol{\psi}(\Im(\boldsymbol{\xi})))\right),$$

with respect to the constraints of workspace as well as the kinematical and actuation constraints. For serial manipulators several approaches have been presented, which use different trajectory parameterization ([9]). The optimization criterion (10) in case of PKM is very challenging, see [10], [21] which is mainly due to the strong workspace constraints. Minimal slopes and tilting of the tool platform yield important reduction of the workspace. Using polynomial approach for optimal input design, such it is known from serial manipulators leads to huge computational effort and do not guarantee convergence or satisfying minimization of the condition number κ. However, the approach presented in [10] has been successfully adapted for the dynamics of parallel kinematics. The excitation trajectories consist of a finite sum of harmonic sine and cosine functions in a form of a finite Fourier series. They can be expressed in cartesian frame, since they present the minimal or general coordinates

$$f_{t,i}\left(x_i, t, \xi^i\right) =$$

$$x_i(t) - x_0^i - \sum_{k=1}^{n} \left(\frac{\mu_k^i}{k\omega_f} \sin\left(k\omega_f t\right) - \frac{\nu_k^i}{k\omega_f} \cos\left(k\omega_f t\right) \right) \tag{10}$$

Each general coordinate x_i corresponds to an appropriate trajectory parameter vector:

$$\boldsymbol{\xi}^i = \left[x_0^i, \ \mu_1^i, \ \cdots \ \mu_n^i, \ \nu_1^i, \ \cdots \ \nu_n^i \right]^T. \tag{11}$$

The fundamental pulsation ω_f of the Fourier series is the same for all degrees of freedom. Thus the trajectory is periodic with a period of $T_f = 2\pi / \omega_f$. The vector of all trajectory parameters $\boldsymbol{\xi}$ groups $\boldsymbol{\xi}^i$ and the fundamental

pulsation ω_f Its dimension is equal to $6(2n + 1) + 1 = 12n + 7$ and depends only on n, which can be chosen arbitrarily. Figure 5 depicts exemplarily one period of an optimized trajectory.

Indications on the Kinematical Computation

A further challenging point about the dynamical identification of complex parallel manipulators is the computation of minimal kinematical variables $\boldsymbol{x}$, $\dot{\boldsymbol{\theta}}$, $\ddot{\boldsymbol{\theta}}$. The minimal coordinates are generally obtained by numerically solving the direct kinematics, see [11].

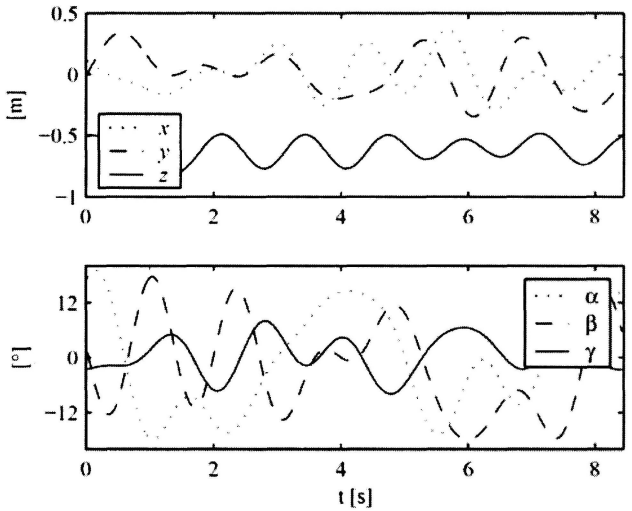

Figure 5: Example of An Optimized Excitation Trajectory in Cartesian Displacements (above) and Tilting Angles (below)

Conventionally, the computation of velocities and accelerations is done by numerical differentiation ([8], [9]). This yields in most of cases to important accumulation and amplification of numerical and measurement errors ([10]). The assumption of noise poor $\boldsymbol{\psi}$ is not maintainable any more. Thus, it is recommended to apply the methods suggested in [9] and [10]. Since the trajectory is available analytically, see equ. (11), the time derivatives can be determined. By means of the forward kinematics, the obtained data $\boldsymbol{x}$ is approximated by a finite Fourier series with the same form as the desired motion given by equ. (11). The parameters of the measured trajectory $\hat{\boldsymbol{\xi}}$ are estimated by applying LS-estimation and inserted in the time derivatives in order to obtain $\dot{\boldsymbol{\theta}}$ as well as $\ddot{\boldsymbol{\theta}}$. The efficiency and precision of the approach were demonstrated using experimental data in [18].

Application to the Hexapod PaLiDA

The presented algorithms are applied to the Hexapod PaLiDA, an innovative Stewart-Gough- platform which was developed by the Institute of Production Engineering and Machine Tools at the Leibniz University of Hannover, see [6]. The identified models are validated by a lot of different trajectories. The close agreement of measured and modeled actuator forces proves the capacity of the presented approach. The application to model-based feedforward control yields significant reductions of tracking errors. Figure 6 shows the tracking errors of actuator 4 during a circular trajectory with a diameter of 0.3 m and endeffector path velocity of 1 m/s. The largest tracking errors are already reduced by the rigid-body model without friction. These deviations occur at the beginning and the end during acceleration and deceleration phases. However, the deviations during constant velocity phase still remain. These errors are reduced after incorporation of the friction model. For the same trajectory, Cartesian path errors are also investigated by computing numerically the direct kinematics. As an example the results are also shown in Figure 6 for strut 4.

In analogy to the actuator errors, the implementation of the identified model yields excellent reductions of path errors, see Figure 7.

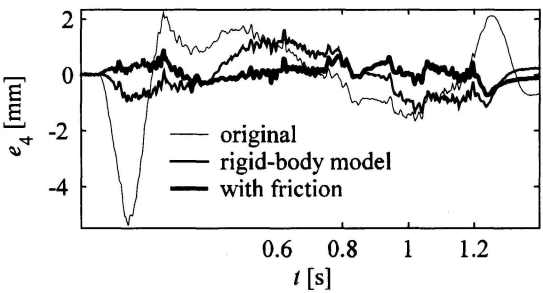

Figure 6: Reduction of Control Errors By Model-Based Feedforward Control for a Circular Trajectory (for example: strut 4 of PaLiDA).

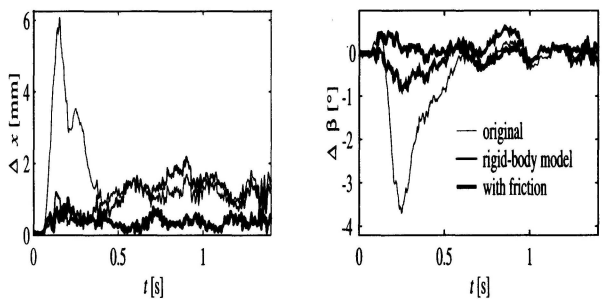

Figure 7: Improvement of Positioning Accuracy by Model-Based Feedforward Control for a Circular Trajectory.

Iterative Learning Control (ILC)

It was noticed that despite the feedforward compensation of nonlinear dynamics and the accurate identification of its parameters, some tracking errors still remain, see [19]. This is due to non-modelled effects and electromagnetic actuator disturbances, primarily. To further increase the control quality, it is opted for applying ILC on the parallel highly coupled mechanism, which is rather a new application in parallel robotics.

Furthermore, it is questionable that the use of direct drives does allow a simple formal decoupling of the complex MIMO-system into multiple SISO-systems. This is demonstrated to be acceptable only in the case of conventional industrial robots or mechanisms, where high gear ratios are used ([16], [17], [21]).

In order to implement linear iterative learning approaches on parallel and therefore highly coupled systems a centralized control architecture has to be provided, i.e. feedforward or feedback computed force control. The consideration of time-variable inertia effects of the actuator can be also used for further decoupling-control of the system, see [22].

The actuators are equipped with conventional PD-controllers, whereas an additional feedforward-compensation of the nonlinear dynamics takes place. Therefore, the ILC is used to decrease the tracking errors of the closed-loop feedback controlled system.

Basics and Design of ILC

The practicability and appropriateness of two ILC methods for PKM have been compared. Approach 1 is based on filtered and phase-lead compensated integral learning ([16], [19]). This algorithm is called sometimes heuristic, since it is not based on an explicit plant model, see [15]. Its implementation is very practical and its design is intuitive and exploits experimentally collected information. In contrast, approach 2 is designed based on explicit knowledge on the system and its transfer dynamics, see [12]. Hereby, the contraction-mapping is chosen. It is interesting to compare both algorithms, in order to find out, if explicit modelling has benefits as suggested in [15]. Firstly, preliminaries on ILC are introduced in the following.

A system is supposed that achieve the same repetitive task over and over. A general SISO or MIMO linear discrete-time system can be described by the state space notation

$$\begin{aligned} \boldsymbol{x}(k+1) &= \boldsymbol{A}(k)\boldsymbol{x}(k) + \boldsymbol{B}(k)\boldsymbol{u}(k) + \boldsymbol{\omega}_1(k) \\ \boldsymbol{y}(k) &= \boldsymbol{C}(k)\boldsymbol{x}(k) + \boldsymbol{\omega}_2(k), \end{aligned} \tag{12}$$

with $\boldsymbol{u}$ being the input and $\boldsymbol{y}$ the output. It is assumed that $\boldsymbol{w}_{1,2}$ represents some deterministic disturbances that appear every repetition as well as measurement disturbances. The system is supposed to be under feedback control, such that equ. (12) describes the closed-loop dynamics.

The aim of ILC is to change the command input every trial j using the learning control law

$$\boldsymbol{u}_{j+1}(k) = \boldsymbol{f}_L(\boldsymbol{u}_j(k), \boldsymbol{y}_j(k), \boldsymbol{y}_d(k)), \tag{13}$$

such that the desired trajectory y_d is tracked as follows

$$\lim_{j\to\infty} \left\| \boldsymbol{y}_j(k) - \boldsymbol{y}_d(k) \right\| = 0. \tag{14}$$

Iterative Learning Control is called linear, when the learning law $\boldsymbol{f}_L$ makes an iterative change in the input that is a linear combination of the error $\boldsymbol{e}_j = \boldsymbol{y}_j - \boldsymbol{y}_d$ measured in the previous repetition and the last input sequence $\boldsymbol{u}_j$:

$$\boldsymbol{u}_{j+1} = \boldsymbol{u}_j + \boldsymbol{L}\boldsymbol{e}_j. \tag{15}$$

The matrix of learning gains L has to be designed in a further step to achieve desired convergence properties or stability. It is simple to derive the iterative error dynamics as

$$\boldsymbol{e}_{j+1} = (\boldsymbol{I} - \boldsymbol{P}\boldsymbol{L})\boldsymbol{e}_j, \tag{16}$$

where $\boldsymbol{I}$ is the identity matrix and

$$\boldsymbol{P} = \begin{bmatrix} \boldsymbol{CB} & \boldsymbol{0} & \cdots & \boldsymbol{0} \\ \boldsymbol{CAB} & \boldsymbol{CB} & \cdots & \boldsymbol{0} \\ \vdots & \vdots & \ddots & \\ \boldsymbol{CA}^{N-1}\boldsymbol{B} & \boldsymbol{CA}^{N-2}\boldsymbol{B} & \cdots & \boldsymbol{CB} \end{bmatrix}, \tag{17}$$

with N being the length of the desired trajectory or input. Most important design criteria of ILC are stability conditions and convergence behaviour of the controller presented by the entries of the matrix $\boldsymbol{L}$. Given the error dynamics in the iteration domain (16), it is obvious that asymptotic stability is achieved, when all eigenvalues of $\boldsymbol{I} \bullet \boldsymbol{PL}$ are less then 1. More relevant from the application point of view and practice is the monotonic decay of error $\boldsymbol{e}$ over the trials. Longman proposed very popular and practical criteria for monotonic convergence of tracking errors, see [16]. It is based on a frequency domain analysis of the system. Assuming that the matrix $\boldsymbol{L}$ is lower triangular, so that it is generated by a causal difference equation (16) can be transformed to

$$\boldsymbol{E}_{j+1}(z) = (\boldsymbol{I} - z\boldsymbol{\phi}(z)\boldsymbol{G}(z))\boldsymbol{E}_j(z), \tag{18}$$

where $G(z) = C(zI - A)^{-1}B$ denotes the transfer function corresponding to L. The substitution of $z = exp\{j\omega T\}$ yields the frequency transfer function. The condition

$$\left|1 - e^{j\omega T}\phi\left(e^{j\omega T}\right)G\left(e^{j\omega T}\right)\right| < 1 \qquad (19)$$

$$\forall\ \omega = 0 \ldots \omega_{Nyquist}$$

assures monotonous decay of the amplitude of all frequencies up to the Nyquist-frequency ([16], [19]). The simplest design of ILC is achieved by selecting the learning matrix to be a diagonal matrix: $L = \Phi I$ (i.e. for MIMO-Systems). It is well-known and proven, that such approach is characterized by bad learning transients at high frequencies ([12], [13], [16]). Even if mathematical convergence is guaranteed, the control error increases remarkably before decreasing to zero, see [16]. To cope with this problem, following two approaches are presented for ILC.

A. Design of Phase-Lead Compensated ILC

The use of a low-pass zero-phase non causal filter f to cutoff the high frequencies improves the performance of the ILC. Additional phase-lead compensation increases the learning bandwidth of the algorithm. The learning control law (15) becomes

$$u_{j+1}(k) = u_j(k) + \Phi_1 f\left(e_j(k+1+l)\right), \qquad (20)$$

where L characterizes the linear phase-lead compensation.
Obviously, zero-error convergence is not possible any more, even in the noise-free case due to the information filtering. This approach needs the adjustment of three parameters: the learning gain Φ_1, the cutoff frequency of the low-pass filter ω and the phase-lead l. This adjustment can be achieved experimentally ([16], [19]) by investigation of the closed loop system dynamics in the frequency domain. In our case a 10th order Butterworth filter was used. The learning parameters are adjusted according to the investigated frequency-response of the closed-loop feedback control system that can be done by simulation or the real system. The error evolution according to the control law (20) in the frequency domain can be derived as

$$E_{j+1}(z) = \left(I - z^{1+l}\Phi_1 F(z) G(z)\right) E_j(z), \qquad (21)$$

that modifies the condition of monotonic error decay (19) to

$$\left|1 - \Phi_1 e^{j(1+l)\omega T} F\left(e^{j\omega T}\right) G\left(e^{j\omega T}\right)\right| < 1, \qquad (22)$$

where F is the filter-transfer function.

For seek of clarity we consider now a single axis of the robot as a SISO system with a measured frequency response $G(e^{j\omega T})$ and the case of zero-phase-lead ($l = 0$). The tuning of ω_c and Φ_1 by examining Nyquist-plots of $G_\Phi = \Phi_1 e$

$^{j(1+l)\omega T}\boldsymbol{G}$ with arbitrarily chosen amplification $\boldsymbol{\Phi}_l$, e.g. $\boldsymbol{\Phi}_l = \boldsymbol{G}^{-1}(\omega = 0)$ and $\boldsymbol{G}$ being an estimate or measurement of the real frequency response (see Figure 8). It is obvious that the monotonic error decay condition (22) is valid for all frequencies for which the plot remains within the unit-circle (centered at +1). The maximal possible cut-off frequency corresponds to the frequency when the Nyquist-plot leaves the unit circle the first time.

The described approach based on conditions (19) and (22) is based on the approximation of the closed-loop dynamics by the linear presentation of the frequency response. The parallel manipulator is characterized by its nonlinear and coupled dynamics, even by the presence of feedforward compensating controller, see [21]. Furthermore, the frequency response based on transient condition (19) assumed that the system reaches steady-state frequency response after the transients [16]. To account for these approximations, as well as for errors while investigating the frequency response, the cutoff frequency is chosen as $\omega_c = 1/2\omega_{max}$, which has been proven for the application in our case to be reasonable (see Figure 8). The linear phase lead helps to increase the learning bandwidth.

It is very simple to deduce from equ. (22), for the same gain $\boldsymbol{\Phi}_l$ and in the case of $l > 0$ the Nyquist-plot leaves the unit circle at a higher frequency. One makes Nyquist-plots of $\boldsymbol{G}$ for a range of integer phase leads and picks the value that keeps the plot less than 1 up to the highest frequency.

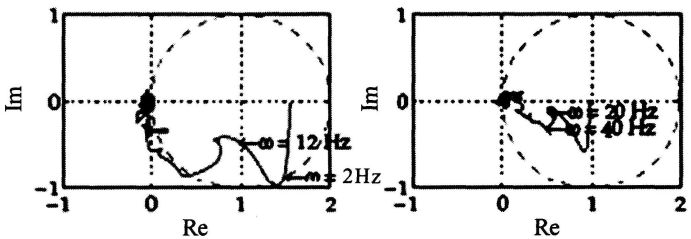

Figure 8: Nyquist-plot for the Tuning of Learning Bandwidth, left: F_l =1.6 or w_{max} = 2 Hz; right: F_l = 1 Hz or w_c = 0.5 w_{max} = 20 Hz.

B. Design of Contraction-Mapping Based ILC

Contraction mapping ILC defines the learning matrix $\boldsymbol{L} = \boldsymbol{\Phi}_l \boldsymbol{P}^T$, where $\boldsymbol{P}$ is the Toeplitz matrix defined by (17). In contrast to the first approach, explicit and parametric system knowledge is required here in form of the matrix $\boldsymbol{P}$. Again, the asymptotic stable feedback controlled MIMO-system is approximated by decoupled linear time invariant LTI-SISO systems. In such case, $\boldsymbol{P}$ contains the values of the impulse response *g(k)*

$$\boldsymbol{P} = \begin{bmatrix} g(1) & & & \\ g(2) & g(1) & & \\ \vdots & \vdots & \ddots & \\ g(N) & g(N-1) & \cdots & g(1) \end{bmatrix}. \tag{23}$$

Experimental investigations determine an optimal ARMAX-structure of the actuators model. The respective model parameters can be identified using standard procedures, see [22]. Hence, the impulse response can be computed and inserted in equ. (23). A filtering is not necessary for the contraction-mapping ILC. Therefore, a zero-error convergence can be achieved theoretically. A further difference to approach 1 is that the condition on monotonic error decay can be derived in the iteration domain by claiming an exact Euclidean norm decay condition

$$\left\| \boldsymbol{e}_{j+1} \right\|_2 < \left\| \boldsymbol{e}_j \right\|_2. \tag{24}$$

It yields by regarding (16)

$$\left\| \left(\boldsymbol{I} - \boldsymbol{PL} \right) \boldsymbol{e}_j \right\|_2 < \left\| \boldsymbol{e}_j \right\|_2, \tag{25}$$

or

$$\left\| \left(\boldsymbol{I} - \boldsymbol{PL} \right) \right\|_2 < 1. \tag{26}$$

Since $\boldsymbol{L} = \boldsymbol{\Phi}_1 \boldsymbol{P}^{\mathrm{T}}$ and the spectral norm of the symmetric matrix $\boldsymbol{PP}^{\mathrm{T}}$ is equal to its maximal eigenvalue $\sigma_{\max}$ one obtains

$$\begin{aligned} &\left\| \left(\boldsymbol{I} - \boldsymbol{PL} \right) \right\|_2 = \max_i \left| \boldsymbol{I} - \boldsymbol{\Phi}_1 \sigma_i \left(\boldsymbol{PP}^T \right) \right| < 1 \\ &\Rightarrow -1 < 1 - \boldsymbol{\Phi}_1 \sigma_{\max} \left(\boldsymbol{PP}^T \right) < 1, \end{aligned} \tag{27}$$

and therefore a rule for the learning gain $\boldsymbol{\Phi}_1$ that allows monotonic error decay

$$0 < \boldsymbol{\Phi}_1 < \frac{2}{\left\| \boldsymbol{P} \right\|_2^2}. \tag{28}$$

In analogy to the first approach it is aware about the restrictive assumption of the LTI-SISO modeling that provides advantageous, since it makes the application of efficient linear ILC possible ([12], [15]). It is reminded here, that the feedback-controlled parallel manipulator is equipped with a feedforward control that compensates the time-variant nonlinear and coupled dynamics ([17], [18], [21]).

The resulting closed-loop error dynamics remains nonlinear, of course. However, their amplitudes are much smaller, that legitimates a linear and decoupled approach. To account for remaining model uncertainties it is convenient to choose a significant smaller gain than the allowed upper bound given by (28).

Simulation Study

The proposed approaches are studies on an accurate model simulation of the parallel robot, which includes rigid-body, friction dynamics, exogenous disturbance forces and parametric and measurement uncertainties. Two trajectories are chosen to be evaluated. The first one is a horizontal quadratic trajectory in the middle of the workspace (z = 0.65 m, length of side d = 0.28 m). The second trajectory is a circular one with a radius of 0.2 m and is also situated at the same height. For both trajectories convergence has been investigated.

The evaluation of the tracking error can be done by the means of a weighted Root-Mean-Square- or RMS-Criteria defined for the complete system and not for single actuators as

$$e_{RMS} = \sum_{i=1}^{6} \left(\sqrt{\frac{1}{N} \sum_{k=1}^{N} \left(q_{d,i}(k) - q_i(k) \right)^2} \right). \tag{29}$$

The results are illustrated in Figure 9.

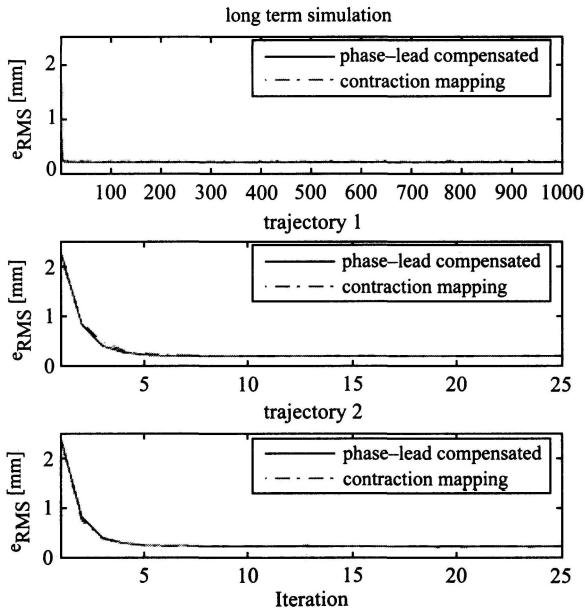

Figure 9: Convergence of the RMS-error: Simulation Study of the Two Investigated Approaches

Both ILC-algorithms show similar performance. The RMS-error converges after a few iterations to a fix value. The long term study did not reveal any divergence which is very satisfactory. The influence of measurement noise is also investigated. For the first trajectory, the ILC procedure was repeated with different measurement white noise level w_2. The normal noise case corresponds to the estimated disturbances of the real system.

The results illustrated in Figure 10 show that convergence rate remains for different disturbance levels equal, whereas the magnitude of the final error increases at higher noise level. As theoretically expected even in the noise-free case, zero-tracking can not be achieved for zero-filtered ILC due to the loss of information.

The contraction mapping did not reach zero-tracking either, but this is due to the structural and parametric uncertainties of the used ARMAX-model. Next result investigated in the simulation is the study on the influence of the compensation of the nonlinear coupled dynamics. Both approaches can deal with coupled dynamics. The used SISO-assumption is therefore admissible. As it is depicted in Figure 11 the same RMS-error level is reached in the case when no inverse model of the robot is compensated (decentralized control case). Of course, the convergence speed is inferior to the case of compensated dynamics (centralized control case). Minor difference remains when using contraction mapping.

This can be explained, that the ARMAX-model is a less accurate approximation of the dynamics in the case, when no compensation of nonlinearities is used.

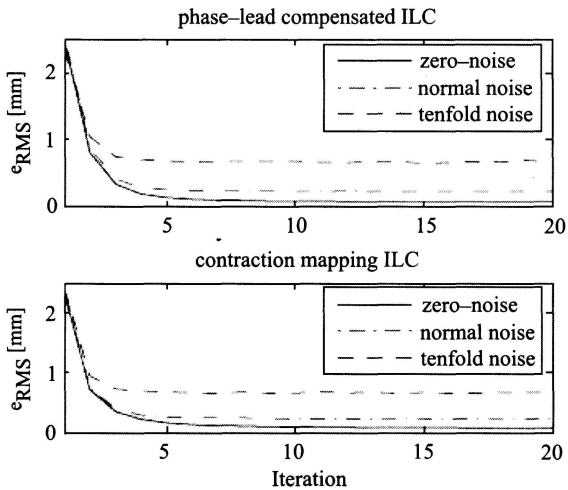

Figure 10: Convergence of the RMS-error in Presence of Different Measurement Noise Levels (Simulation Results).

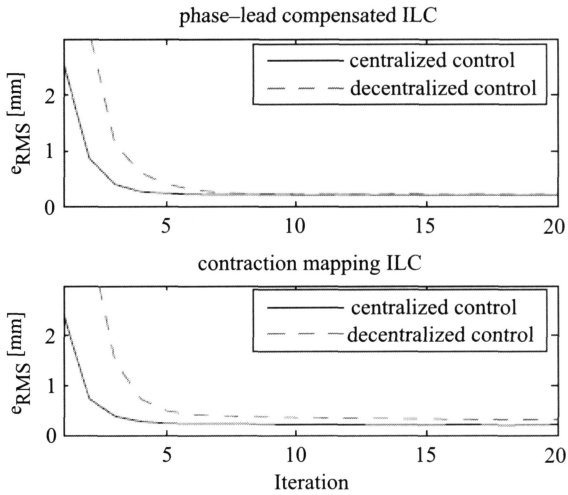

Figure 11: Influence of the Control Architecture on Learning Performance

Finally, periodograms have been used to illustrate the remaining tracking error after the 20th ILC-trial. The spectral density of the tracking errors of one arbitrarily chosen actuator are compared with the related initial errors. Figure 12 demonstrates clearly the success of ILC for the attenuation of the tracking errors about at least 30dB at low frequencies (< 50Hz). Both validated approaches were successful and are comparable in their performance.

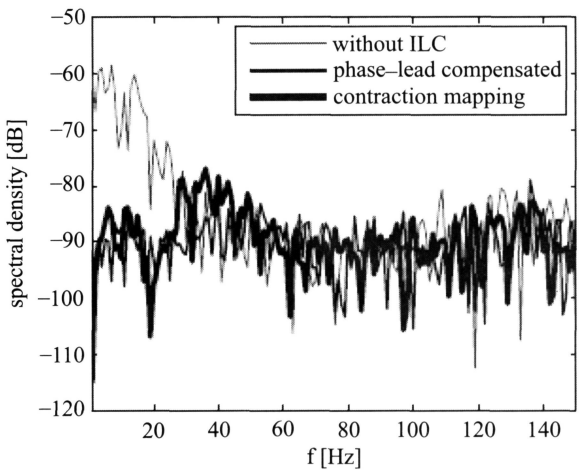

Figure 12: Spectral Densities of Tracking Errors in Simulation: Without ILC, After 20 Iterations of Phase-lead Compensated ILC and After 20 Iterations of Contraction Mapping

Experimental Results

After the simulation study ILC was performed on the real system. The parallel robot is controlled with a commercial board which is a dSPACE Power-PC 604e (333 MHz). Only internal Hall-sensors are used for measuring the actuator lengths. Unfortunately, these sensors are reputed by being very noisy, see [17]. Figure 13 shows a comparison of the RMS error over the trials for the two approaches and for the two investigated trajectories.

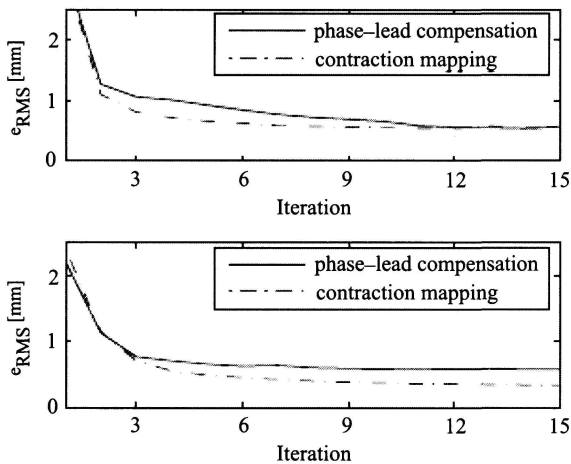

Figure 13: RMS-error Convergence for the Parallel Robot, Up:Quadratic Motion, Down:Circular Motion.

Besides similar convergence behaviour, the contraction-mapping approach seems to be more advantageous on the real system. This can be explained, that the approximation of the nonlinear dynamics of the real manipulator with the linear frequency response is less accurate than the dynamics modelling using ARMAX equations.

It demonstrates the improvement of the tracking performance, achieved by both tested approaches. The examination of the corresponding spectral densities of the control errors (see Figure 14) affirms that in the practical case, contraction mapping ILC yields more improvement of control accuracy. This is observed especially for low (< 10Hz) and high frequencies (> 50Hz).

The time histories of the tracking errors are depicted for an exemplarily chosen actuator 4 in Figure 15.

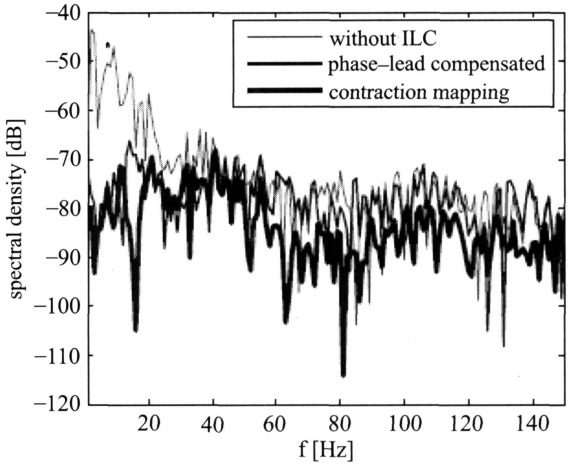

Figure 14: Spectral Density of Tracking Errors in Experiments: Without ILC, After 20 Iterations of Phase-lead Compensated ILC and Contraction Mapping Method ILC

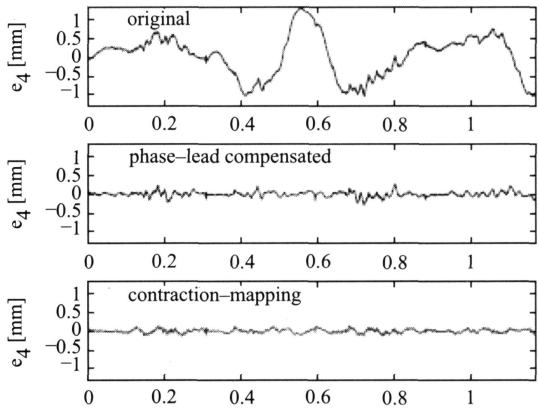

Figure 15: Remaining Tracking Error of Actuator 4 by Using Feedforward Control (up), After Phase-lead Compensated ILC (middle) and After Contraction-mapping ILC (Down)

Conclusions

In this paper an approach is presented that makes the identification of the dynamics of complex parallel mechanisms possible. The presented identification method of the dynamical parameters for parallel manipulators is based on a direct approach. Hereby, only single optimised trajectories are needed for well conditioned measurements and therefore good estimation results. This paper

also proposed iterative learning control (ILC) for enhancing tracking performance of a parallel direct driven manipulator. The promising results have shown that simple linear ILC approaches were sufficiently applied to achieve important improvement despite the nonlinear coupled dynamics of the system. A phase-lead compensated algorithm and a contraction-mapping based approach were compared first in a simulation study, than by experiment on the real system.

Acknowledgments

The authors would like to thank the German Research Foundation (DFG) for the financial support of our work and the Institute of Production Engineering and Machine Tools of the Leibniz University of Hanover for the provision of the hexapod robot PaliDA for experimental investigations.

References

[1] Armstrong, B. (1988). "Dynamics for robot control: friction modeling and ensuring excitation during parameter identification", Ph. D.-thesis, Stanford University, Stanford.

[2] Grotjahn, M., Daemi, M. and Heimann, B. (2001). "Friction and Rigid Body Identification of Robot Dynamics", Int. J. of Solids and Structures, 38(10-13) pp. 1889-1902.

[3] Grotjahn, M., Kühn, J., Heimann, B. and Grendel, H. (2002). "Dynamic Equations of Parallel Robots in Minimal Dimensional Parameter-Linear Form", Proc. of the 14th CISM-IFToMM Symposium on the Theory and Practice of Robots and Manipulators (RoManSy2002), pp. 67-76.

[4] Honegger, M., Brega, R. and Schweitzer, G. (2000). "Application of a Nonlinear Adaptive Controller to a 6 dof Parallel Manipulator", Proc. of the IEEE Int. Conf. on Robotics and Automation, pp. 1930-1935.

[5] Sirouspour, M.R. and Salcudean, S.E. (2001). "Nonlinear Control of a Hydraulic Manipulator", Proc. of the IEEE Int. Conf. on Robotics and Automation, pp. 3760-3765.

[6] Tönshoff, H.K., Grendel, H. and Grotjahn, M. (2002). "Modelling and Control of a Linear Direct Driven Hexapod", Proc. of the Int. Conf. on Parallel Kinematical Machines, pp. 335-350.

[7] Zhang, C.D. and Song, S.M. (1993). "An efficient method for inverse dynamics of manipulators based on the virtual work principle", J. of Robotic Systems, 10(5), pp. 605-627.

[8] Grotjahn, M., Heimann, B. and Abdellatif, H. (2004). "Identification of Friction and Rigid-Body Dynamics of Parallel Kinematical Structures for Model Based Control", Multibody Systems Dynamics 11(2004), pp. 273-294.

[9] Severs, J., Gansemann, C., de Schutter, J. and van Brussel, H. (1996). "Experimental Robot Identification Using Optimised Trajectories", Journal of Mechanical Systems and Signal Processing. 5(10), pp. 561-577.

[10] Abdellatif, H., Benimelli, F., Heimann, B. and Grotjahn, M. (2004). "Direct Identification of Dynamic Parameters for Parallel Manipulators", Proc. of the Int. Conference on Mechatronics and Robotics 2004, MechRob2004, Aachen, Germany, pp. 999-1005.

[11] Merlet, J.-P. (2000). "Parallel Robots, Solid Mechanics and its Applications", Kluwer Academic Publishers. Doderecht, The Netherlands.

[12] Longman, R.W. (2003). "On the interaction between theory, experiments, and simulation in developing practical learning control algorithms", International Journal of App. Math. Computer. Sciences., Vol. 13, no. 1, pp. 101-111.

[13] Bien, Z. and Xu, J.-X. (Eds.) (1998). "Iterative Learning Control, Analysis, Design, Integration and Applications". Boston/Doderecht/London: Kluwer Academic Publishers.

[14] Moore, K.L. (1999). "Iterative learning control: An expository overview," Applied and Computational Control, Signals and Circuits, vol. 1, pp. 151-214..

[15] Norrlöf, M. and Gunnarsson, S. (2002). "Experimental results of some classical iterative learning control algorithms," IEEE Transactions on Robotics and Automation, vol. 18, no. 4, pp. 636-641.

[16] Elci, H., Longman, R.W., Phan, M.Q., Juang, J.-N. and Ugoletti, R. (2002). "Simple learning control made practical by zero-phase filtering: Applications to robotics," IEEE Transactions on Circuits and Systems-I: Fundamental Theory and Applications, vol. 49, no. 6, pp. 753-767.

[17] Denkena, B., Heimann, B., Abdellatif, H. and Holz, C. (2005). "Design, modeling and advanced control of the innovative parallel manipulator palida," in Proc. of the IEEE/ASME Int. Conference on Advanced Intelligent Mechatronics, AIM2005, Monterey, USA, pp. 632-637.

[18] Abdellatif, H., Grotjahn, M. and Heimann, B. (2005). "High efficient dynamics calculation approach for computed-force control of robots with parallel structures," in Proc. of the 44th IEEE Conference on Decision and Control, CDC-ECC05, Seville, Spain, pp. 2024-2029.

[19] Ye, Y. and Wang, D. (2003). "Better robot tracking accuracy with phase lead compensated ILC," in Proc. of the IEEE Int. Conference on Robotics and Automation, ICRA2003, Taipei, Taiwan, pp. 4380-4385.

[20] Sciavicco, L. and Siciliano, B. (2000). "Modelling and Control of Robot Manipulators", 2nd Ed. London: Springer.

[21] Abdellatif, H., Heimann, B. and Holz, C. (2005). "Applying efficient computation of the mass matrix for decoupling control of complex parallel manipulators," in Preprints of the 16th IFAC World Congress, Prague, Czech Republic.

[22] Lung, L. (1999). "System Identification: Theory for the User", 2nd ed. Upper Saddle Hall, New Jersey: Prentice-Hall.

JOURNAL OF MECHANICAL ENGINEERING (JMechE)

Aims & Scope

Journal of Mechanical Engineering (formerly known as Journal of Faculty of Mechanical Engineering), is an international journal which provides a forum for researchers and academicians worldwide to publish the research findings and the educational methods they are engaged in. This Journal acts as a vital link for the mechanical engineering community for rapid dissemination of their academic pursuits as well as a showcase of the research activity of FKM for the outside world.

Contributions are invited from various disciplines that are allied to mechanical engineering. The contributions should be based on original research works. An attempt will be made to review the submitted contributions with competent internal and external reviewers as to the suitability of the paper for satisfying the objectives of the journal.

All papers submitted to JMechE are subjected to a rigorous reviewing process through a worldwide network of specialized and competent referees. To be considered for publication, each paper should have at least two positive referee's assessments.

General Instructions

Manuscripts intended for publication in the Journal FKM should be written in camera ready form with production-quality figures and done electronically in Microsoft Word 2000 (or above) and submitted along with one hard copy. Manuscripts should be typed using Times New Roman font (point 10) on one side of the paper (A4 size), single-spaced, with wide margins (1 in left and right, and 1 in on top and bottom). The manuscript should include the title of the paper; the author's name and affiliation; a short abstract of between 200 and 300 words which clearly summarises the paper; and a list of keywords. Limit your submission to a maximum of 20 typed pages.

Keywords

Keywords supplied by the author should appear on a line following the abstract. The keywords selected should be comprehensive and subject specific. Maximum of five keywords should be sufficient to cover the major subjects of a given paper. General terms should not appear as keywords, as they have little use as information retrieval tools. Please choose keywords to be as specific as possible and list the most specific first, proceeding to the most general last.

Units

All scientific and technical data presented should be stated in SI units.

Footnotes

Footnotes should be kept to an absolute minimum and used only when essential.

Formulae

Formulae should be typewritten using MS Word compatible Equation Editor.

Tables

Tables, should be included within the text where appropriate and must be numbered consecutively with Arabic numerals and have titles that precede the table. They should be prepared in such a manner that no break is necessary.

Figures

Authors should appreciate the importance of good-quality illustrations. All graphs and diagrams should be referred to, for example, Figure 1 in the text. All figures must be numbered consecutively with Arabic numerals. A detailed caption should be provided below each figure according to the following format:

Figure 1: (a) A simple 2-D cantilever and (b) microcantilever with a diamond probe.

Figures should be embedded within the text where appropriate. Glossy photographs when required should be scanned to a resolution suitable with the reproduction requirements (1200 dpi generally will be sufficient).

References

Use squared brackets to indicate reference citation such as [1], [3]-[5] in the main text. Include references at the end of the paper according to the citations order that appears in the paper using the following format.

[1] M. K. Ghosh and A. Nagraj, "Turbulence flow in bearings," Proceedings of the Institution of Mechanical Engineers 218 (1), 61 - 64 (2004).

[2] H. Coelho and L. M. Pereira, "Automated reasoning in geometry theorem proving with Prolog," J. Automated Reasoning 2 (3), 329-390 (1986).

[3] P. N. Rao, Manufacturing Technology Foundry, Forming and Welding, 2nd ed. (McGraw Hill, Singapore, 2000), pp. 53 – 68.

[4] Hutchinson, F. David and M. Ahmed, U.S. Patent No. 6,912,127 (28 June 2005).